RSC Advances

PAPER

View Article Online
View Journal | View Issue

Cite this: *RSC Adv.*, 2017, **7**, 48263

Differentiating the impact of nitrogen chemical states on optical properties of nitrogen-doped graphene quantum dots†

Timothy Pillar-Little and Doo Young Kim *

Received 21st August 2017
Accepted 8th October 2017

DOI: 10.1039/c7ra09252k

rsc.li/rsc-advances

The optical properties of top-down synthesized oxidized graphene quantum dots (ox-GQDs) and nitrogen-incorporating graphene quantum dots (N-GQDs) along a range of hydrothermal treatment temperatures were observed. By controlling the hydrothermal treatment temperature, different chemical states of nitrogen atoms were incorporated into GQDs. Below 150 °C, edge-terminating amines and amides dominated the nitrogen content of N-GQDs. Above 150 °C, nitrogen was primarily present in the forms of pyridinic, pyrrolic and quaternary N. In addition to the absorbance and emission profiles of ox-GQDs and N-GQDs, pH-dependent emission spectra were collected to probe chemical states of nitrogen atoms and investigate the relationship between nitrogen location and photoluminescence.

Graphene quantum dots (GQDs) are the newest member in the functional carbon nanomaterials family. The unique combination of a sp^2-carbon nanodomain and edge-terminating functional groups of GQDs offers facile routes to surface passivation and functionalization as well as tunable band-gap properties. Due to their high surface-to-volume ratio and defect-rich chemical structure, GQDs are utilized in a broad range of applications including optoelectronics, electro- and photocatalysis, and biological therapeutics.

A number of methods have been employed to produce GQDs, including chemical oxidation,[1–3] electrochemical preparation,[4] hydrothermal cutting,[5] and electric arc method.[6] Despite the variety of synthetic methods, top-down synthesized GQDs contain large sp^2-hybridized carbon planes with some defects such as holes or heteroatoms. The optical band gap of GQDs is determined by (i) the dimension of GQDs and (ii) surface states of GQDs. The surface states of GQDs can be modified by introducing heteroatoms at defects or attaching surface functional groups.[7–10] GQDs are a promising alternative for a variety of applications such as bioimaging,[11] photodynamic therapy,[12] wound disinfection,[13] heavy metal sensing,[14] electrocatalysis,[15] and photovoltaic devices.[16] In contrast to other nanomaterials, GQDs are significantly more biocompatible than other types of carbon nanomaterials such as carbon nanotubes, graphene, and graphene oxide.[17,18]

Nitrogen is one of the most studied elements as a dopant for the host carbon nanomaterial as the introduction of nitrogen atoms perturbs electrostatic charge of adjacent carbon atoms. Recent literature demonstrates the red-shifted emission of nitrogen-containing GQDs which is attributed to the reduction of the band gap[7,8] Additionally, the incorporation of nitrogen atoms into a sp^2 carbon framework in the bottom-up synthesis of GQDs has also shown the increase of photoluminescence quantum yield (PLQY). Interestingly, these dopants have also been reported to induce the blue shift of emission due to the strong electron affinity of nitrogen atoms which invokes a partial positive charge on adjacent carbon atoms.[19,20] Aside from optical properties, doping nitrogen heteroatoms into carbon nanomaterials shows a great enhancement of the electrocatalytic activity toward the oxygen reduction reaction (ORR).[19]

Recently, Tetsuka *et al.* reported that absorption/emission properties of amino-functionalized GQDs were finely tuned by controlling hydrothermal temperature from 70 °C to 150 °C.[7] In this report, the shift of spectral position and the enhancement of fluorescence intensity were mostly attributed to N-related surface functionalities such as primary amines and amides. However, the role of edge-terminating nitrogen sites, *i.e.*: pyridines and pyrroles, and core N sites such as quaternary N were largely neglected. The maximum content of nitrogen atoms was observed at the lowest hydrothermal temperature and the content of nitrogen became reduced as the temperature was raised.[7] In support of these experimental observations, a recent computational work likewise shows the quantity of amine N is connected to the red-shifted behavior of GQDs.[8] In contrast to the Tetsuka study, a recent article brought about the importance of pyridinic, pyrrolic and quaternary N sites. This study employed much higher hydrothermal temperatures (>150 °C) and observed blue-shifted emission with higher quantum yield ($\Phi = 34.5\%$).[9]

Until now, there were very few studies differentiating the effect of different N chemical states (*i.e.*, amines, pyridines,

Department of Chemistry, University of Kentucky, Lexington, KY 40506, USA. E-mail: dooyoung.kim@uky.edu; Tel: +1-859-257-5597

† Electronic supplementary information (ESI) available. See DOI: 10.1039/c7ra09252k

pyrroles) on the optical properties of top-down-synthesized GQDs. However, a recent work by Qu *et al.* has shown a pronounced differentiation of pyrrolic and graphitic N states in the bottom-up synthesized carbon nanodots.[21] This report utilizes the hydrothermal dehydration of urea and citric acid to show a direct correlation between the quantity of graphitic N and increase of PLQY. In addition, varying the nitrogen source from urea to ethylenediamine greatly enhanced the PLQY to 94%. Carbon nanodots made in this way have also been employed as fluorescent probes for *in vitro* and *in vivo* studies with excellent cellular uptake and biocompatibility in mice.[22]

In the present study, hydrothermal temperature was controlled as an effective method to incorporate different chemical states of nitrogen atoms into GQDs. Four different chemical states of nitrogen atoms (amine, pyridinic, pyrrolic, and quaternary) were identified and related to absorption/emission properties. Moreover, pH-dependent emission spectra was studied to probe chemical states of nitrogen atoms and to investigate the relation between nitrogen location and emission.

The synthesis of oxidized GQDs (ox-GQDs) and the subsequent nitrogen incorporation (N-GQDs) are described in Fig. 1a. ox-GQDs were prepared by reacting 100 mg of carbon nano-onions with a 1 : 3 ratio of concentrated H_2SO_4 : HNO_3 under 95 °C reflux and vigorous stirring for 4 hours. The reaction was terminated when the reflux solution became clear and brownish in color. Afterwards, this solution was first centrifuged at 4000 rpm for 90 minutes to allow the precipitation of unreacted carbon nano-onions. Then, the supernatant was neutralized with K_2CO_3 and dialyzed for 6 days with a dialysis bag (1 kDa MWCO) to remove excess ions from the neutralization. After dialysis, the resulting solution contains the purified ox-GQD in water. N-GQDs were prepared by reacting ox-GQDs with NH_4OH in a hydrothermal reactor, as similar to the report by Tetsuka *et al.*[7] First, ox-GQDs were mixed with 5.0 M NH_4OH (1 : 2 v/v). The mixture was then placed into a 200 mL stainless steel autoclave reactor for 5 hours. The hydrothermal temperature of the reaction was varied from 90–190 °C. N-GQD-X prepared at a specific temperature such as 150 °C will now be referred as N-GQD-150.

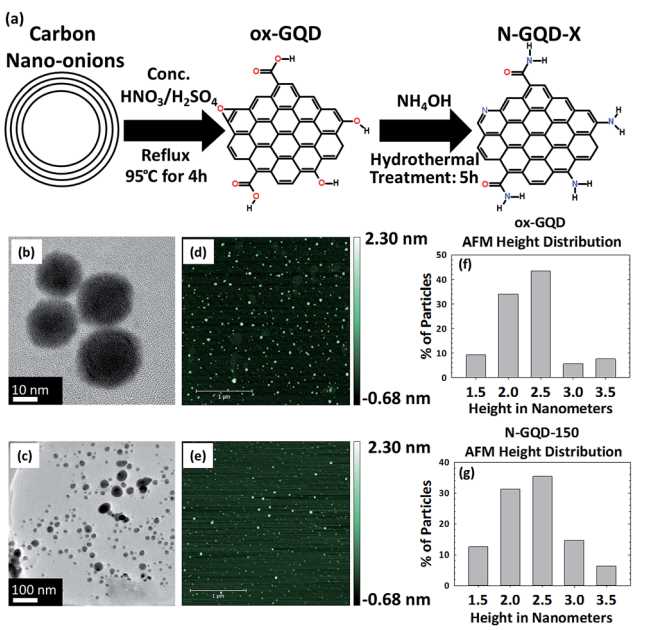

Fig. 1 (a) A scheme for the synthesis of GQDs and N-GQDs. TEM images of ox-GQD (b) and N-GQD (c), AFM images of ox-GQD (d) and N-GQD (e), and the histogram of the thickness of ox-GQDs (f) and N-GQDs (g).

Morphology and chemical structure are important factors to determine the optical behaviour of ox-GQDs and N-GQDs. The size and the thickness of ox-GQDs and N-GQDs were characterized by TEM (JEOL JEM-2200FS, 200 kV) and atomic force microscopic (AFM) characterizations (Park Systems XE-70). The results of TEM and AFM characterizations are shown in Fig. 1b–g. The size of ox-GQDs varies from 20–30 nm. As the functional groups are modified, electrostatic interactions and hydrogen bonding may induce some amount of aggregation which can be seen for N-GQDs. AFM characterization of ox-GQDs and N-GQDs revealed isolated particles. As shown in the histogram (Fig. 1f and g), both ox-GQD and N-GQD show an average thickness of 2.5 nm, indicating that both particles are made of multiple stacks of graphene nanosheets.[24]

Hydrothermal temperature (90–190 °C) greatly influenced the chemical functionalities and the incorporated nitrogen atoms in N-GQDs prepared. The chemical structure of N-GQDs and chemical states of nitrogen incorporated were probed by FT-IR and XPS analyses. FT-IR spectra were recorded with a Thermo Scientific Model Nicolet 6700 FT-IR Spectrometer and are displayed in Fig. S1.† As shown in Fig. S1,† FT-IR spectra of ox-GQD exhibited the presence of hydroxyl, carbonyl and carboxyl groups located at 1000 cm^{-1} (C–O), 1700 cm^{-1} (C=O), 2500 cm^{-1} (CO_2H) and 3300 cm^{-1} (–OH), respectively. Compared to ox-GQDs, a new peak appeared at 1070 cm^{-1} in N-GQD-150, which is assigned to C–N bond. In addition, the peak at 1700 cm^{-1} became broadened due to the overlay of amide and carbonyl C=O. The carboxylic acid peak at 2500 cm^{-1} was suppressed in N-GQD-150, supporting the conversion of carboxylic group into amine or amide. Most notably, the broad peak at 3300 cm^{-1} in ox-GQD due to hydrogen bonded O–H stretching became much narrower in N-GQD, indicating the substitution of hydroxyls to primary and secondary amines.

XPS characterization was conducted with a Thermo Scientific Model K-Alpha XPS instrument. The high resolution spectra were deconvoluted using Avantage software by Thermo Scientific. Peak position for each chemical state is detailed in the main text as well as in Table S1.† XPS analyses were conducted after drying of GQD solution mounted on a silicon wafer. Fig. 2a shows hypothetical structure of N-GQDs where nitrogen atoms are incorporated into various sites. The nitrogen-incorporated sites include pyridinic N (398.5 eV, N1), amine N (399.7 eV, N2), pyrrolic N (400.2 eV, N3), and quaternary N (401.3 eV, N4). N 1s peaks were assigned according to the NIST Standard Reference Database.[27] The assignments of XPS peaks to different chemical states by previous studies and this report are summarized in the ESI (Table S1†).

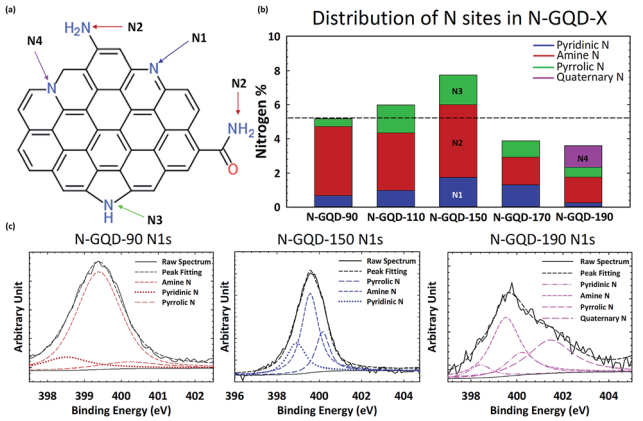

Fig. 2 (a) A simplified representation of nitrogen-incorporated GQDs. The four chemical states of nitrogen are listed as N1 (pyridinic), N2, (amine/amide), N3 (pyrrolic) and N4 (quaternary or graphitic). (b) The percentage of N chemical states in N-GQDs determined by N1s high resolution XPS spectra. The average nitrogen content (5.3 ± 1.7%) is denoted by the dashed line. (c) High resolution XPS N1s spectra of N-GQD-90, N-GQD-150 and N-GQD-190.

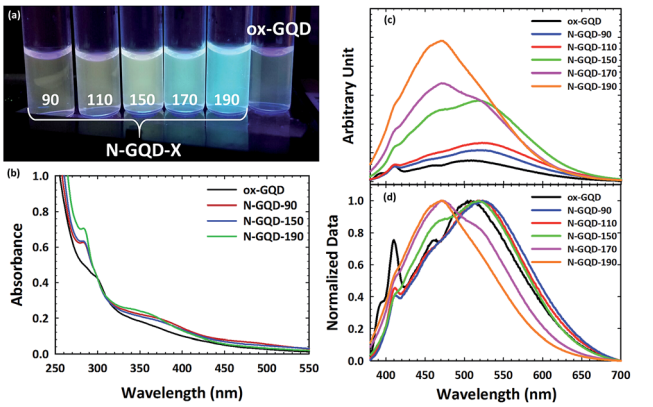

Fig. 3 (a) The photograph of ox-GQDs and N-GQDs under a UV lamp (364 nm exc) (from left: N-GQD-90, N-GQD-110, N-GQD-150, N-GQD-170, N-GQD-190, and ox-GQD). (b) UV-visible absorbance, (c) emission spectra, and (d) normalized emission spectra of ox-GQDs and N-GQD-90, N-GQD-110, N-GQD-150, N-GQD-170, and N-GQD-190. Emission spectra of GQDs were taken at $\lambda_{ex} = 360$ nm.

Fig. 2c shows the high resolution XPS N1s peaks of N-GQDs synthesized at N-GQD-90, N-GQD-150, and N-GQD-190. The high resolution XPS N1s peaks of N-GQDs were deconvoluted to resolve the relative fraction of N1, N2, N3 and N4. While N-GQD-90 and N-GQD-150 are mainly deconvoluted with N1, N2, and N3, the N-GQD-190 showed the significant fraction of N4 (quaternary N). Fig. 2b shows the evolution of the relative fraction of N1–N4 sites present in N-GQDs synthesized at different hydrothermal temperature. Clearly, the total N content of N-GQDs increased from 5% to 8% when hydrothermal temperature was raised up to 150 °C. Then the content of N went down at 170 °C and 190 °C. The reduction of nitrogen content for N-GQD-170 and N-GQD-190 is likely due to the hydrothermal cutting of ox-GQD, as consistent with the results reported by Luo *et al.*[25] Overall, the content of amine groups (N2) tends to go down as temperature becomes higher. On the other hand, the content of other types of N edge sites such as pyridinic (N1) and pyrrolic (N3) rises until the temperature reaches 150 °C. At temperatures above 150 °C, the relative fraction of pyridinic N and pyrrolic N decrease. These N sites are converted to quaternary N in N-GQD-190.

Optical properties of GQDs and N-GQDs are strongly influenced by the functional groups found in the edge structure. Absorption spectra were recorded with a Thermo Scientific Evolution 201 Spectrophotometer and Emission spectra were recorded with a Jobin-Yvon Spectromax 4 Spectrofluorometer. The excitation-dependent PL spectra for ox-GQD, N-GQD-90, N-GQD-150, and N-GQD-190 are shown in Fig. S2.† Fig. 3a shows the photograph of GQDs and N-GQDs dispersed in water under UV lamp ($\lambda = 365$ nm). While N-GQD-90 and N-GQD-150 show green to yellow emission, N-GQD-170 and N-GQD-190 exhibited much stronger blue emission.

Fig. 3b presents UV-VIS absorption spectra of ox-GQDs and N-GQDs. The UV-Vis absorption spectra display three bands (300 nm, 370 nm, and 470 nm). The 300 nm peak of ox-GQDs is assigned to the π–π* transition and it is shifted to 280 nm in N-GQDs. This blue-shift is attributed to the strong electron affinity of nitrogen atoms, which were reported to enhance the delocalization of electrons in the graphene nanodomain.[9,10] The peak at 370 nm is prominent for all N-GQDs and it is assigned to the n–π* transition. This 370 nm band is shifted to shorter wavelength (350 nm) upon the increase of hydrothermal treatment temperature. This particular band is attributed to the effect of non-bonding orbitals from pyridinic N and pyrrolic N as previously described by Li *et al.*[10] Lastly, the absorbance band at 470 nm that relates to another surface state n–π* transition tends to become weaker as the hydrothermal temperature gets higher. The 470 nm band is likely due to the amine N and shows the maximum absorbance in N-GQD-90, as shown in a previous report.[7] From these results, the different surface states associated with pyridinic N, pyrrolic N, and amine N show their individual impact on the absorption profile of the NGQD. It should also be noted that hydrothermal temperature-dependent evolutions of UV-VIS spectra are consistent with nitrogen-related chemical states revealed in the XPS analysis discussed above.

Fig. 3c shows the emission spectra of ox-GQD and N-GQDs. Emission spectra were taken at excitation wavelength of 360 nm. As can be seen, emission intensity gradually increases as the hydrothermal temperature was raised. There are two major bands observed in the emission spectra of N-GQDs: 470 nm and 525 nm. Compared to ox-GQD, N-GQD-90 and N-GQD-110 show the red-shift of emission from 500 nm to 525 nm. The 525 nm emission is attributed to the surface state associated with amine N sites. N-GQD-150 shows the emergence of a prominent new band at 470 nm. This band is related to the maximal content of pyrrolic N.[10] For N-GQD-170, the emission at 525 nm is suppressed; however, the emission at 470 nm is greatly enhanced. Based upon the results of XPS analysis, the 470 nm emission comes primarily from pyrrolic N, while the 525 nm emission is related to the amine N sites. N-GQD-190

shows the emission enhancement at 470 nm is even greater and is assigned to the addition of quaternary N. The increased emission intensity at 470 nm follows a similar trend to the previously mentioned work by Qu *et al.*[21] As in that report, our results likewise show that the presence of pyrrolic N and quaternary N strongly contributes to the enhanced PLQY. More details on the measured PLQY can be found in the ESI.† Overall, the samples which were hydrothermally treated at low temperatures contain large concentrations of amine and pyridinic N and displayed red-shifted emission profiles. Conversely, high hydrothermal treatment temperatures drive nitrogen addition toward pyrrolic and quaternary N sites. These absorption and emission results clearly demonstrate the resolved energetics of four different N-related chemical states in N-GQDs.

In order to further probe surface functionalities of GQDs and N-GQDs, the emission of ox-GQD and N-GQDs was explored as a function of pH. The effects of tuning the quantity of carboxylic acids and phenols have been studied by Mei *et al.*[23] and Luo *et al.*[25] Both functional groups were found to promote non-radiative processes with red-shifted emission. Although pH-dependence of GQDs and polyethylene glycol (PEG)-modified GQDs were reported by Zhu *et al.*[26] and Jin *et al.*,[8] N-GQDs with primary amines/amides, pyridinic, *etc.* toward the change of pH has been rarely reported. In ox-GQDs, the pH-sensitive functional groups are carboxylic acids ($pK_a \sim 5$) and phenols ($pK_a \sim 10$). Fig. 4a shows the pH dependence of ox-GQDs shows a similar trend as previous reports.[8,26] Major pH-induced changes observed for ox-GQDs are the enhancement of emission intensity from pH = 5 to pH = 7 and the suppression of emission intensity from pH = 7 to pH = 9. While pH influences the emission intensity of ox-GQD, a slight shift of emission position was also observed. The spectral position change is clearly coupled with the protonation/de-protonation of carboxylic acids and phenols around their respective pK_a values. The origin may be due to either the variation of absorption cross-section in the formed charged species or non-radiative interaction with environment. The normalized emission spectra in Fig. 4b show slightly red-shifted emission maxima with increasing pH which can also be linked to additional non-radiative processes such as collisional quenching.

Fig. 4c and d show the pH dependent emission of N-GQD-150. The most pronounced change in PL intensity is the significant emission enhancement at 520 nm from pH 5 to pH 7. Little change is observed above pH 7. This change of emission intensity is attributed to protonation/deprotonation of either pyridine N or amine N sites which both have a $pK_a \sim 5$. The contrast between ox-GQDs and N-GQD-150 clearly indicates the difference in surface chemistry of the two GQDs. As reported in the work by Luo,[25] hydrothermal treatment removes hydroxyl groups, so little change in PL intensity above pH 7 is expected. The different behaviour of the emission peaks at 460 nm and 520 nm indicates that the two peaks have different origins. The normalized PL spectra of N-GQD-150 (Fig. 4d) show the red-shift of emission as the pH changes from 5 to 7.

The PL spectra of N-GQD-190 (Fig. 4e and f) shows the pH dependence similar to that of N-GQD-150, but to a lesser extent. This is likely due to the reduced total content of nitrogen in N-GQD-190, along with the smallest quantity of pH-sensitive functional groups (amine and pyridine) among all N-GQD samples. The origin of the emission around 470 nm in N-GQD-150 and N-GQD-190 is hypothesized as pyrrolic and quaternary nitrogen. These two functional groups have a negligible pH dependence in aqueous media, so the 470 nm emission would be unaffected by pH change. The enhanced emission intensity at pH > 7 is due to the contribution of 520 nm emission coming from amine and pyridinic N sites. As can be seen in Fig. 4e and f, N-GQD-190 also shows the red-shifted emission maxima but to a lesser degree due to its smaller quantity of amine and pyridinic N sites.

The results herein clearly demonstrate the relation between nitrogen-related surface states and emission property. Overall, with the increase of the hydrothermal temperature, the amount of pyridinic and pyrrolic nitrogens relative to amine nitrogen is enhanced. The total content of nitrogen atoms was found to be maximal at 150 °C. At lower temperatures, amine groups were predominant as a result of a kinetically-favored addition of aqueous ammonia. At higher temperature, surface amines are converted to edge-sites (pyridinic or pyrrolic), core N sites (quaternary), or partially removed signifying a thermodynamically favourable process. These results clearly differentiate the impact of N chemical states on optical behaviour of GQDs. This understanding is critical for developing finely tuned, high-performance nanoparticles that are also more environmentally-friendly. Fundamentally understanding the effects that specific nitrogen chemical states have on carbon nanomaterials will bolster their potential use in optoelectronics, bioimaging, photo- and electrocatalytic applications.

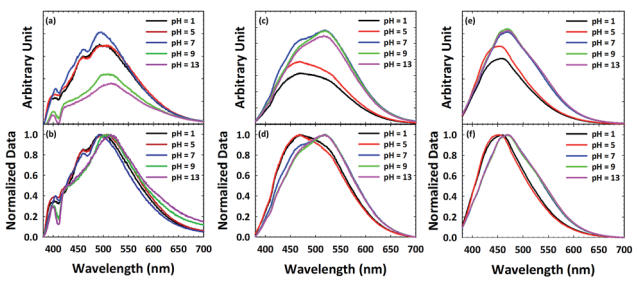

Fig. 4 Emission spectra of (a and b) ox-GQD, (c and d) N-GQD-150 and (e and f) N-GQD-190 excited with 360 nm light plotted as a function of pH.

Conflicts of interest

There are no conflicts to declare.

Acknowledgements

The authors thank Prof. Ambrose Seo and John Connell for AFM characterization. The authors appreciate Dali Qian for TEM characterizations. This work was supported by the National Science Foundation under Cooperative Agreement No. 1355438. The purchase of a new XPS system recently installed at the

University of Kentucky was supported by the fund from the NSF EPSCoR grant (grant no. 0814194).

Notes and references

1 J. Peng, W. Gao, B. K. Gupta, Z. Liu, R. Romero-Aburto, L. Ge, L. Song, L. B. Alemany, X. Zhan, G. Gao, S. A. Vithayathil, B. A. Kaipparettu, A. A. Marti, T. Hayashi, J. J. Zhu and P. M. Ajayan, *Nano Lett.*, 2012, **12**, 844.
2 Y. Dong, C. Chen, X. Zheng, L. Gao, Z. Cui, H. Yang, C. Guo, Y. Chi and C. M. Li, *J. Mater. Chem.*, 2012, **22**, 8764.
3 H. Tao, K. Yang, Z. Ma, J. Wan, Y. Zhang, Z. Kang and Z. Liu, *Small*, 2012, **8**, 281.
4 D. B. Shinde and V. K. Pillai, *Chem.–Eur. J.*, 2012, **18**, 12522.
5 D. Pan, J. Zhang, Z. Li and M. Wu, *Adv. Mater.*, 2010, **22**, 734.
6 M. Bottini, C. Balasubramanian, M. I. Dawson, A. Bergamaschi, S. Bellucci and T. J. Mustelin, *J. Phys. Chem. B*, 2006, **110**(2), 831.
7 H. Tetsuka, R. Asahi, A. Nagoya, K. Okamoto, I. Tajima, R. Ohta and A. Okamoto, *Adv. Mater.*, 2012, **24**, 5333.
8 S. H. Jin, D. H. Kim, G. W. Jun, S. H. Hong and S. Jeon, *ACS Nano*, 2013, **7**(2), 1239.
9 Y. Dai, H. Long, X. Wang, Y. Wang, Q. Gu, W. Jiang, Y. Wang, C. Li, T. H. Zeng, Y. Sun and J. Zeng, *Part. Part. Syst. Charact.*, 2014, **31**, 597.
10 Y. Li, Y. Zhao, H. Cheng, Y. Hu, G. Shi, L. Dai and L. Qu, *J. Am. Chem. Soc.*, 2012, **134**, 15.
11 S. Zhu, J. Zhang, C. Qiao, S. Tang, Y. Li, W. Yuan, B. Li, L. Tian, F. Liu, R. Hu, H. Gao, H. Wei, H. Zhang, H. Sun and B. Yang, *Chem. Commun.*, 2011, **47**, 6858.
12 Z. M. Markovic, B. Z. Ristic, K. M. Arsikin, D. G. Klisic, L. M. Harhaji-Trajkovic, B. M. Todorovic-Markovic, D. P. Kepic, T. K. Kravic-Stevovic, S. P. Jovanovic, M. M. Milenkovic, D. D. Milivojevic, V. Z. Bumbasirevic, M. D. Dramicanin and V. S. Trajkovic, *Biomaterials*, 2012, **33**, 7084.
13 H. Sun, N. Gao, K. Dong, J. Ren and X. Qu, *ACS Nano*, 2014, **8**(6), 6202.
14 H. Sun, N. Gao, L. Wu, J. Ren, W. Wei and X. Qu, *Chem.–Eur. J.*, 2013, **19**, 13362.
15 Q. Li, S. Zhang, L. Dai and L. Li, *J. Am. Chem. Soc.*, 2012, **134**(46), 18932.
16 Y. Li, Y. Hu, Y. Zhao, G. Shi, L. Deng, Y. Hou and L. Qu, *Adv. Mater.*, 2011, **23**, 776.
17 X. Zhang, Y. Zhu, J. Li, Z. Zhu, J. Li, W. Li and Q. Huang, *J. Nanopart. Res.*, 2011, **13**, 6941.
18 C. Wu, C. Wang, T. Han, X. Zhou, S. Guo and J. Zhang, *Adv. Healthcare Mater.*, 2013, **2**, 1613.
19 K. Gong, F. Du, Z. Xia, M. Durstock and L. Dai, *Science*, 2009, **323**(5915), 760.
20 S. Y. Wang, D. S. Yu and L. M. Dai, *J. Am. Chem. Soc.*, 2011, **133**, 5182.
21 D. Qu, M. Zheng, L. Zhang, H. Zhao, Z. Xie, X. Jing, R. E. Haddad, H. Fan and Z. Sun, *Sci. Rep.*, 2014, **4**, 5294.
22 M. Zheng, S. Liu, J. Li, Z. Xie, D. Qu, X. Miao, X. Jing, Z. Sun and H. Fan, *J. Mater. Res.*, 2015, **30**, 3386.
23 Q. Mei and Z. Zhang, *Angew. Chem., Int. Ed.*, 2012, **51**, 5602.
24 D. Pan, J. Zhang, Z. Li and M. Wu, *Adv. Mater.*, 2010, **22**, 734.
25 P. Luo, Y. Qiu, X. Guan and L. Jiang, *Phys. Chem. Chem. Phys.*, 2014, **16**, 19011.
26 S. Zhu, J. Zhang, X. Liu, B. Li, X. Wang, S. Tang, Q. Meng, Y. Li, C. Shi, R. Hu and B. Yang, *RSC Adv.*, 2012, **2**, 2717.
27 A. V. Naumkin, A. Kraut-Vass, S. W. Gaarenstroom and C. J. Powell, *NIST Standard Reference Database 20, Version 4.1*, 2012.